POLISH POLAR RESEARCH
vol. 45 no. 1, pp. 1–19 DOI: 10.24425/ppr.2023.146738

Grounding line positions of Amery Ice Shelf based on long interferometric Sentinel-1 time series

Michał TYMPALSKI*, Marek SOMPOLSKI, Anna KOPEĆ and Wojciech MILCZAREK

Faculty of Geoengineering, Mining and Geology, Wrocław University of Science and Technology, ul. Na Grobli 15, 50-421 Wrocław, Poland

** corresponding author <michal.tympalski@pwr.edu.pl>*

Abstract: The paper presents the potential of combining satellite radar data and neural networks for quasi-automatic detection of glacier grounding lines. The conducted research covered five years and was carried out in the area of the Amery Ice Shelf. It has a very complex shoreline, so its grounding-line location is uncertain. Thus, it has always been the subject of much research. The main objective of our work was to find out if Synthetic Aperture Radar data combined with a deep learning implementation would enable rapid detection of ice shelf grounding lines over large areas. For this purpose, 290 radar images from the Sentinel-1 satellite covering 46 000 km^2 were used. Processed by the Differential Interferometry of Synthetic Aperture Radar four-pass method, the images formed a time-consistent series between 2017 and 2021. As a result of performed calculations, a total length of 1280 km of grounding line was determined. They were validated by comparing with other independent data sources based on manual measurements. It has been demonstrated that the combination of satellite radar data and automated data processing allows for obtaining high-precision results continuously in a very short time. Such an approach allows monitoring of grounding line position in the long term with intervals of less than one week. It enables analysis of the dynamics changes with unprecedented frequency and the identification of patterns.

Keywords: Antarctic, Prydz Bay, ice shelf, DInSAR, CNN.

Introduction

Antarctica, the most extensive ice depository in the world, is a critical area, specifically in the light of current climate changes. The boundary between the grounded ice sheet and the free-floating ice shelf, called grounding line, has particular importance for the cryosphere monitoring. The grounding line is defined as the border at which the ice loses contact with the seafloor and becomes a freely drifting ice shelf (Weertman 1974). In reality, its location is in constant variation, which depends, *e.g.*, on tides, wave action, and ice thickness, so the grounding line is in fact a zone several kilometers wide (Fricker and Padman 2006). Fricker *et al.* (2009) pointed out that the grounding line position was one of the typical parameters to monitor the changes and stability of ice shelves. It is an essential component of cryosphere research, providing insights into mass balance perturbations, interactions between ice shelves and ice sheets, and factors affecting glacier recession (Tsai and Gudmusson 2015; Brondex *et al.* 2017). The primary difficulty in accurately determining the grounding line is its location under the glacier cover, thus measurements of its position often provide uncertain information or have low precision (Horgan and Anandakrishnan 2006). It is usually determined by manual delineation based on satellite images (Rignot *et al.* 2016), which is a time-consuming process. Considering that each person perceives differently, delineations carried out by two or more individuals might also differ slightly. Depending on such features as humidity, the thickness of the snow cover, and the glacier's geometric properties, the changes in the images can be classified differently. Each glacier also differs in terms of texture, *e.g.*, its roughness and internal structure. Hence, these techniques require much knowledge and experience in pattern recognition. Since this process is time consuming, such data is collected only several times per year. The low frequency at which the results are obtained forces extrapolations from a small sample of data for deeper analysis (Straneo *et al.* 2016). This problem poses a challenge in assessing and analyzing seasonal glacier changes (Schild and Hamilton 2013; Catania *et al.* 2018; Fried *et al.* 2018).

Techniques that allow the direct location of the grounding line are mainly based on comparing signal echo patterns, using seismic (Horgan *et al.* 2013, 2017), ground-based (Jacobel *et al.* 1994; MacGregor *et al.* 2011) or aboveground (aerial) (Uratsuka *et al.* 1996) sounding. Other approaches can be classified as indirect since, in their case, the measurement is not strictly around the grounding line, but other features visible on the glacier's surface determine its location. One of the most commonly used traits is the limit of the vertical movements (hinge/flexure line) caused by ocean motion (Holdsworth 1969; Rignot 1996). Although this feature is usually slightly shifted landward relative to the grounding line, it represents a valid approximation (Vaughan 1994; Rignot *et al.* 2011). The term "grounding line" is used in both the direct and indirect methods, even though they result in an accurate determination and approxima-

tion, respectively (Friedl *et al.* 2020). In the past, it was measured mainly by field surveys, *e.g.*, gravimetry (Lambrecht *et al.* 1997), tiltmeter (Stephenson 1984), static (Fricker *et al.* 2002) and kinematic (Vaughan 1994) Global Positioning Systems (GPS), and ground-based photogrammetric time-lapse imagery (Rosenau *et al.* 2013). However, since glaciers are located in remote and inaccessible places, field measurements are costly, time consuming, and often impossible to accomplish.

The situation is different with the use of satellite data, which does not rely on field presence and allows coverage of a much larger area, which is a significant advantage in the case of glacier measurements. Initial studies have shown that tidal methods can measure ice cover and monitor glacier conditions (Goldstein *et al.* 1993; Rignot 1996). Currently, the most widely used methods include Differential Interferometric Synthetic Aperture Radar (DInSAR) (Rignot *et al.* 2011; Milillo *et al.* 2017; Mohajerani *et al.* 2021), Differential Range Offset Tracking (SAR DROT) (Joughin *et al.* 2010; Marsh *et al.* 2013), Repeat Track Laser Altimetry (RTLA) (Fricker and Padman 2006; Brunt *et al.* 2010), and Pseudo Cross-track Radar Altimetry (PCRA) (Bamber *et al.* 2009). An in-depth study of tidal methods used in grounding line measurements had been conducted by Friedl *et al.* (2020), who concluded that for the optimal grounding line detection, identification on DInSAR interferogram was, for the time being, the most accurate.

Grounding line data for the key glaciers in Antarctica are provided by ESA Antarctic Ice Sheet Climate Change Initiative (AIS_cci) project based on ERS 1/2 (1994–1996), TerraSAR-X, and Copernicus Sentinel-1 (2014–2021) satellites (Floricioiu *et al.* 2021). The Making Earth System Data Records for Use in Research Environments (MEaSUREs) project - Antarctic Grounding Line from Differential Satellite Radar Interferometry, Version 2, also provides grounding line data. These data are based on imagery from the ERS 1/2 (1992–1999), Radarsat 1/2 (2000, 2009), PALSAR (2007–2009), COSMO SkyMed (December 2013), and Sentinel-1A (December 2014) satellites (Rignot *et al.* 2016). Both sets result from manual delineations of interferograms obtained by DInSAR method. In both cases, the data are not time consistent, *e.g.*, one measurement per year, and are only available for selected areas. The most recent data set was published by Mohajerani *et al.* (2021), covering the entire Antarctic for 2018 with intervals of 6 and 12 days (depending on Sentinel-1 data availability). They were derived by combining DInSAR method with the Convolutional Neural Network (CNN) for automatic delineation.

The primary purpose of this paper is the identification of grounding lines and zones in a long-time horizon, using SAR data with the four-pass DInSAR method, and the implementation of deep learning for automatic recognition of selected dependencies on interferograms. Combining the multitude of SAR data with the ability to process them automatically allows a solution that monitors the position of the grounding line on a pseudo-continuous cycle, which might be a particularly important aspect of cryosphere monitoring.

Study area

The Amery Ice Shelf is supplied by three glaciers (Fisher, Mellor, and Lambert), which together form the Lambert-Amery glacier system. It is the largest ice shelf in East Antarctica, with an area of around 60 000 km^2 (Galton-Fenzi *et al.* 2008). Figure 1 shows its location in Antarctica, its key features, and the coverage of the used Sentinel-1 data (orbit No.3, frames 834, 839, 844, 849). The chosen orbit and frames cover around 46 000 km^2 of the Amery Ice Shelf, just about 75% of the entire glacier area. This basin drains 16% of the East Antarctic ice sheet (Fricker *et al.* 2002). It is also the northernmost (69°S) ice shelf (Fricker *et al.* 2009). Unlike other Antarctic ice shelves, *e.g.*, Ronne or Ross, the Amery Ice Shelf is in a long, narrow, sub-ice-shelf cavity. In addition, there are no warm currents in its region, making it less exposed to basal melting (Fricker *et al.* 2001; Gwyther *et al.* 2015). On the other hand, its shoreline and grounding line are highly complex. For this reason, the grounding line location of the Amery Ice Shelf has been studied for many years, with the first studies conducted in the late 1960s, based on field surveys (Budd *et al.* 1982). Its position was then redefined based on a numerical terrain model developed using SAR imagery (ERS 1/2), ice thickness, and density model data (Fricker *et al.* 2002). Further determinations of the grounding line alignment in the Amery shelf area are based almost exclusively on satellite data: a combination of InSAR data, optical imagery from the MODIS sensor and laser altimetry data (ICESat sensor) (Fricker *et al.* 2009) as well as integration of optical data (Landsat sensor) and altimetry data (ICESat) (Xie *et al.* 2016).

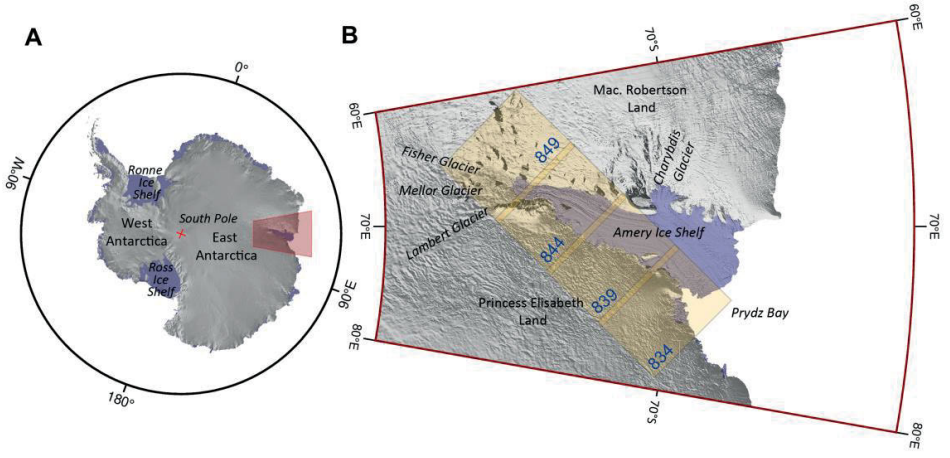

Fig. 1. Location of the Amery Ice Shelf region in East Antarctica (**A**; red tetragon) and the study area (**B**) with four frames from the path No.3 of Sentinel-1 satellite, marked as yellow rectangles with IDs in blue.

Methods

Grounding line delineation. — DInSAR approach is based on the calculation of an interferogram, defined as the difference in signal phase between consecutive satellite acquisitions. It results in vertical and horizontal displacements in the satellite line of sight with topographical and atmospheric influences (Rosen *et al.* 2000; Hanssen 2001). In the case of glacier monitoring, each interferogram is affected by phase shifts, resulting, in addition to surface topography and noise, from the horizontal and steady glacier flow driven by sliding and gravity (Rignot *et al.* 2011). It makes it considerably difficult for grounding line delineation, which only requires information about vertical displacements. For this purpose, double-difference interferograms, which require four acquisitions, are determined (Rignot and MacAyeal 1998). This operation helps to reduce the glacier flow influence, which, combined with the extraction of the topographic phase by using the Digital Elevation Model (DEM), makes it possible to obtain an interferogram consisting only of vertical displacements. These are represented as fringes indicating the difference in phase between two interferograms (Fig. 2), where each range equals a 28 mm motion of the surface

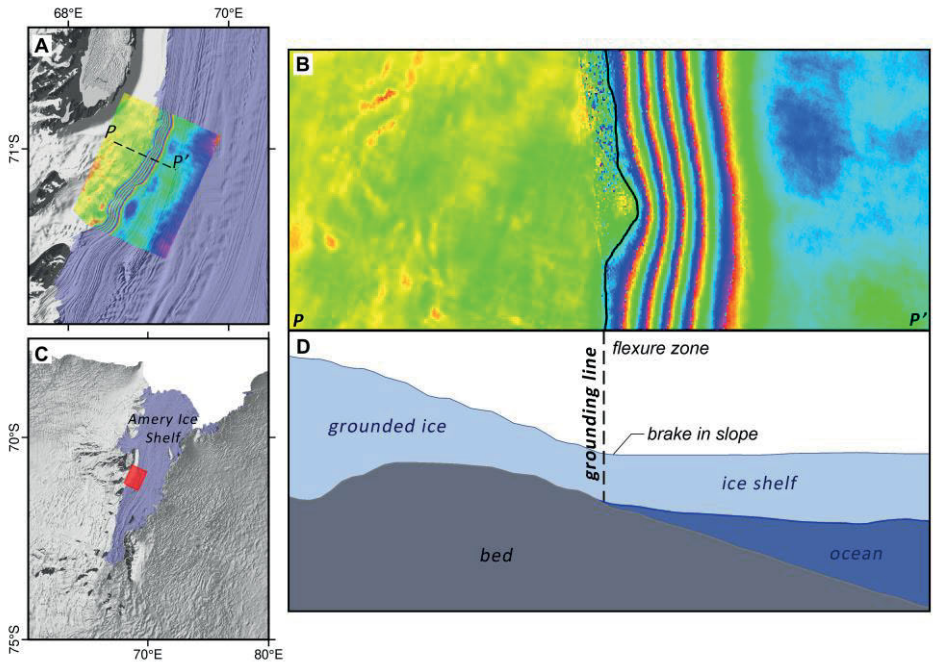

Fig. 2. Illustrative location of the grounding line (**A**, **B**) for a selected area of the Amery Ice Shelf (**C**): (**A**) the placement of the cross-section line superposed on the interferogram, (**B**) the course of the grounding line superposed on the interferogram, and (**D**) the cross-section through the shelf and ice-sheet bedding, based on Bedmap2 database (Fretwell *et al.* 2013).

along the line of sight of the radar. The zone in which the density of the fringes significantly increases imitates the increased vertical motion caused by the movement of the freely drifting ice shelf above the ocean. The most landward one indicates the flexure line (Fricker *et al.* 2009), which is usually very close (*ca.* 100 m) to the grounding line (Rosier *et al.* 2017).

Thanks to its extremely precise determination of vertical displacements of a few cm, depending on wavelength of the sensor, the approximation of the position of the grounding line is currently the most accurate approach. The big advantage of DInSAR is its ability to take measurements over large areas at once. The repeatability of the evaluation with successive satellite acquisition allows the detection of rapid and short-term changes in the position of the grounding line (Rignot *et al.* 2014). In addition, this method does not depend on either weather conditions or time of day. Nevertheless, it requires high coherence between interferograms, which can be disturbed by the rapid movement of the glacier surface and the change in reflection characteristics caused, *e.g.*, by melting of the top layer of ice (Yu *et al.* 2010; Hogg *et al.* 2016). Since this effect increases with the temporal resolution between imaging (Bamler and Hartl 1998), a shorter interval between acquisitions results in better performance. Hence, data availability over a brief period is a crucial limitation of DInSAR method in detecting grounding lines (Friedl *et al.* 2020).

The use of tidal methods such as DInSAR significantly improves capabilities of grounding lines detection. Compared to *in-situ* measurement, it reduces the time needed to achieve results from several months to a few weeks. Further reduction in the timeframe can be achieved only through faster recognition of shapes in images, which would require the involvement of more experts. However, the problem of manually drawn grounding lines will remain the primary factor preventing continuity in receiving results within several days.

Automatic processing. — An alternative approach that allows the identification of factors related to the grounding line in a short time is the usage of neural networks (LeCun *et al.* 2015). Image segmentation techniques have improved rapidly in recent years due to advances in deep learning and semantic image segmentation using Convolutional Neural Networks (CNNs) (Krizhevsky *et al.* 2017). It has been already demonstrated that CNNs can be effectively applied in detecting objects, their changes (Anantrasirichai *et al.* 2018; Huang *et al.* 2020) or classification (Kussul *et al.* 2017). The functioning of the convolutional layer in the network can be described as an operation of multiplying a set of weights (filter) with input. The filter is smaller than the input data, and the type of multiplication applied between a filter-sized patch of the input and the filter is a dot product. Because of the smaller filter size, it is used systematically for each overlapping part or filter-sized patch of the input data, left to right, top to bottom, producing an array of dot products called a feature map (Heaton 2020). With each convolutional layer, different weights of the filter are applied, resulting in the recognition of various features. Additionally, in the

first half of U-Net-based CNNs, max-pooling layers are used to downsample outputs of previous layers, creating smaller images fed into next convolution layers. That operation allows CNNs to detect the finest patterns as well as ones clearly visible on the input image. In the second half, smaller outputs are upsampled and concatenated to consequently yield an image of the same size as the input.

Large amounts of SAR data provided by Sentinel 1 satellite constellation forced the creation of the method of their automated processing. Determining the grounding line position is a target detection problem (same as for calving fronts). Up-to-day, three approaches were developed in that field: based on the most likely path (Mohajerani *et al.* 2021), based on distinguishing between glacial and non-glacial mixtures (Zhang *et al.* 2019), and based on combining information on the altitude and the polarization (Baumhoer *et al.* 2019). These processing methods and the high frequency of image acquisition might enable continuous measurements of glacier dynamics and hence, the condition of the glacier.

Data and its processing. — To delineate the grounding line, radar data from the Sentinel-1 mission were used. With the aim of revealing the potential for pseudo-continuous monitoring of the grounding line position, the measurement period was set for five years (January 2017–December 2021). Since both Sentinel-1 satellites are considered, SAR images are acquired regularly every six days, giving 298 acquisition days. For four frames that gives a total of 1192 Sentinel-1 slices obtained. These are the first such in-depth results for Amery Ice Shelf.

Preparation of the interferogram requires co-registration of scenes (Fig. 3A). First, frames are stitched together to reduce processing time, resulting in one image per day scenario. Next, the images are paired based on a six-day interval to form a continuous time series of pairs, which means that the secondary image from one pair is simultaneously the reference image on the following one. It enables interferogram generation, resulting in a wrapped, filtered phase, corresponding to its shifts between two acquisitions. Extraction of the topographic phase was achieved by ArcticDEM (Porter *et al.* 2018). All the above calculations were performed using GMTSAR software (Sandwell *et al.* 2011). Next, the data are adapted for CNNs prediction (Fig. 3B). Subsequent interferograms are differentiated to remove the glacier flow influences, similar to the pairing process – subtrahend interferogram becomes minuend in the next subtraction. The resulting new interferograms are geocoded and cut into smaller tiles to avoid GPU bottleneck. The maintenance of mutual coverage of 52 px (about 10%) on each side helps avoid edge effects after stitching. As a final input to the network go wrapped, filtered and geocoded phase images of 512×512 px size.

The interferograms are then processed by algorithms for automatic determination and delineation of grounding lines (Fig. 3C). In our case, 40-layer CNN proposed by Mohajerani *et al.* (2021) was used. It was trained based on 252 manually interpreted DInSAR phase and coherence images of Getz Ice

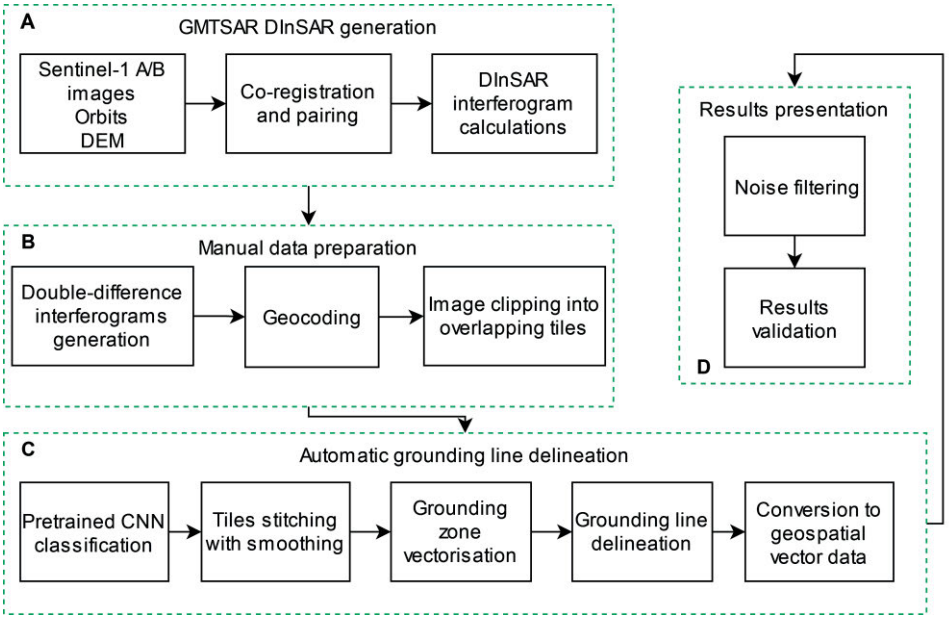

Fig. 3. Data processing flowchart, parts concerning: (**A**) GMTSAR DInSAR generation, (**B**) manual data preparation, (**C**) automatic grounding line delineation, (**D**) results presentation.

Shelf. The result of the network's work on a single tile is a raster with the same dimensions as the input. Output raster pixel values represent the probability of containing grounding lines. A threshold of 30% probability is applied to represent the area of measurement uncertainty. Each image is rebuilt by combining tiles into a full depiction using a Gaussian filter. The resulting features are vectorized and filtered based on perimeter length - a threshold value adopted for 6 km aims to reduce the number of false grounding lines while preserving real objects. Based on the filtered polygons, the centerline is drawn with the use of the label_centerlines Python package. The final step is to merge the resulting objects into a single product, corresponding to the date of acquisition, and convert all files into geospatial vector data. It is important to mention here that the results have not been interfered with in any way, such as manual completion of gaps or extrapolation of trajectory. Having the post-processed outcomes, it is only a matter of manually removing the unnecessary noise features created during processing by verifying them with the expected grounding line position (Fig. 3D).

Results validation. — The results' accuracy was assessed by comparing them with other independent data sources. As mentioned in the introduction, there are two datasets regarding the position of the grounding line around Antarctica – AIS_cci program (Floricioiu *et al.* 2021) and the MEaSUREs project (Rignot *et al.* 2016). According to the latest research, methods that were used to obtain this data are currently the best tools in the context of the grounding line position (Friedl *et al.* 2020), so the accuracy of these data will not be questioned in this paper. Unfortunately, only the AIS_cci dataset coincides to some extent

with the chosen measurement period. Out of the entire set, only the corresponding data were selected. It resulted in ten paired dates for which the measurement periods were identical, eight of which were from 2020. These measurements were from the same year's season, with a frequency equal to the acquisition of one of the Sentinel-1 satellites (six days). Therefore, only results from this period's beginning, middle, and end were selected. Eventually, the comparison was made for five periods, with the addition of single measurements from 2017 and 2019. Note that this is only the difference between delineation performed manually by an expert and automatically by a machine. It does not describe the accuracy of the DInSAR itself or refer to the true grounding line position.

To quantify the differences between manually and automatically delineated grounding lines, the metric based on the PoLiS algorithm (Avbelj *et al.* 2015) was calculated. Proposed metric starts with decomposition of the manually prepared lines into two-point line segments. After that, for each vertex in the automatically delineated data set, the closest segment is being found. Shortest distances between point and segment are summed for each feature and divided by double the number of points. Second part of the metric is the sum of shortest distances between the points in selected segments and lines in automatically prepared dataset, also divided by double the number of points. Both components are calculated individually for each line in the automatically delineated data set. Finally, the components are summed for each line resulting in the validation metric.

Results

General assessment. — The estimated length of the grounding line in the area is 1360 km, with our results covering around 1280 km, which is nearly 95% coverage. An example interferogram resulting from SAR data processing using the DInSAR (four-pass) method (Fig. 4) shows fringe distribution around Amery Ice Shelf. For most areas (1, 2, 5, and 6 on Fig. 4) where the presence of a grounding line is expected, high intensity of the fringes is visible, based on which delineation can be performed. However, some disturbing features have also been observed (areas 3 and 4 on Fig. 4), causing troubles in the delineation process.

Figure 5 shows twelve representative profiles through the grounding zone, separated into summer (October-February in green) and winter (March-September in blue) seasons. Associated with it, Fig. 6 presents the changes in grounding line position for individual profiles, relative to the geometric center (specific to each profile) over time. The minimum and maximum positions of the grounding lines (yellow triangles) are usually located in the middle or at the very end/beginning of the season, barely appearing in the quarters. The movement of these points shows a certain regularity, appearing twice in the middle and once at

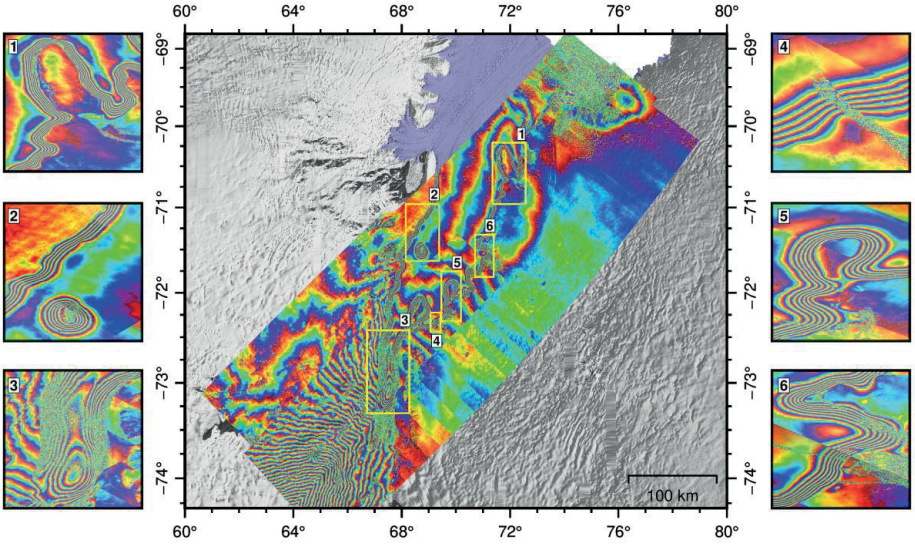

Fig. 4. Results of processing of SAR data from Sentinel-1 satellite in the form of double-difference interferograms for the period 2021.07.24–2021.08.17. Yellow polygons indicate areas for which detailed results are presented. The map is underlain by a numerical terrain model – ArcticDEM (Porter *et al.* 2018), coordinate system EPSG:4326.

the end and the beginning, in a four-season cycle. A large number of observations enabled the identification of migrating grounding zone, defined as the range between the maximum and minimum grounding line positions in each season, *i.e.*, summer marked by blue bars and winter by gray bars. The most significant migration can be observed at the beginning of the floating ice (profiles 3–5), indicating that at some point the grounding line has retreated even 4000 m inland. In most cases, the seasonal extent of the grounding zone settles around 500–1000 m, with the maximum values not exceeding 2000 m. In the case of profiles 8, 9, and 10 (located in the eastern part of the shelf), a seasonal regularity is apparent, indicating a movement of the grounding line toward land in summer and moving away in winter. On the other hand, analyzing the trend, in 2018–2020 the position of the grounding line deviated from the average, most often towards the land (profiles 1, 9–12), by *ca.* 100–200 m. Also clearly observable are the maximum values that the trend line reaches just before the end of winter (profiles 1 and 12) and how, as it moves deeper into the glacier, the maximum retreats relative to the time axis. This phenomenon matches the direction of movement of the glacial masses.

Results validation. — Performing the results validation procedure described in the previous section, the line-to-line distances were obtained. The mean metric values between automatically and manually delineated lines varies from 302 to 565 m in the analyzed period. Higher mean values are observed for regions where higher decorrelation and noise were observed. In such places more outliers occur

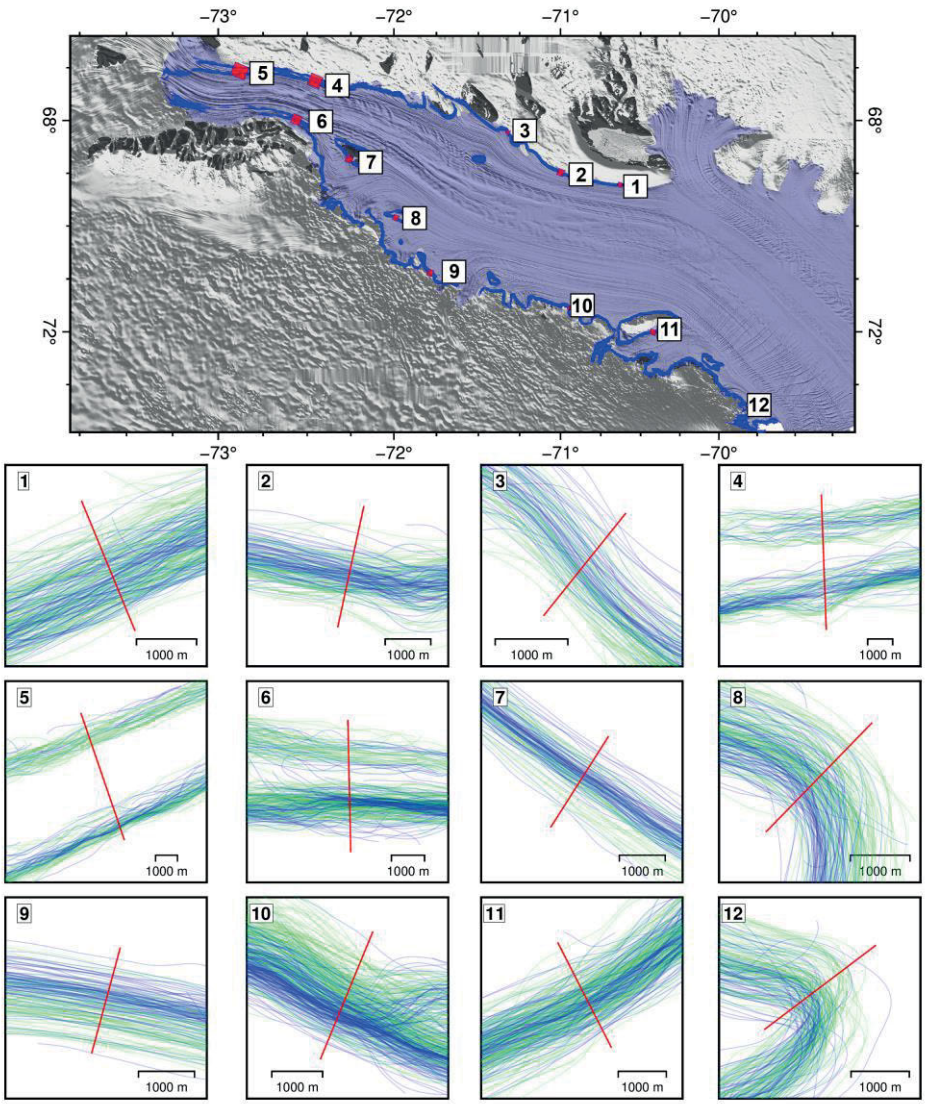

Fig. 5. Results of detected grounding lines for 12 sections located in selected areas of the Amery Ice Shelf (map on the top). The red color indicates the course of the sections. The blue lines refer to grounding lines detected in winter, and the green refer to the ones detected in summer. The map is underlain by the numerical terrain model – ArcticDEM (Porter *et al.* 2018), WGS 84/Antarctic Polar Stereographic (EPSG:3031) coordinate system.

influencing the mean value of delineation error. The median values are more evenly distributed around 300 m for each date. Considering that mean values are much lower than the precision of the second most precise method, which is RTLA (*ca.* 0.5–1 km precision) (Friedl *et. al.* 2020), the results were evaluated as reliable.

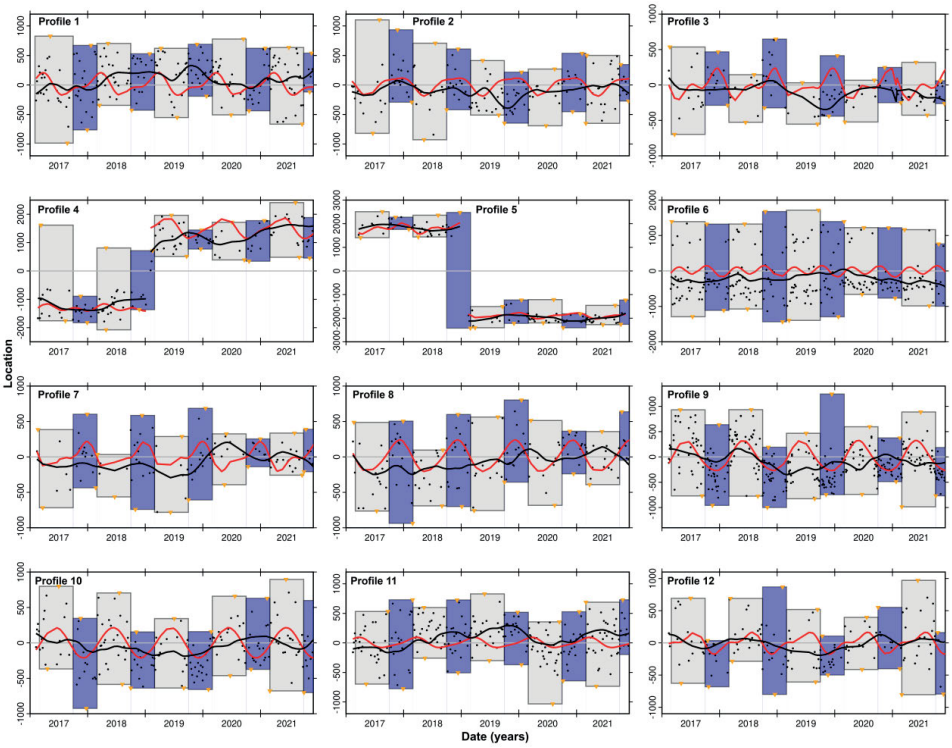

Fig. 6. Analysis of seasonality and long-term trend of grounding line migration for the entire period. The black points on each graph represent the intersection of detected grounding lines along a given profile (see Fig. 5). For each profile, the zero value on the Y-axis was determined independently and represents the geometric center of the set of intersection locations of consecutive grounding lines along the profile. Seasonality is shown in red, and the long-term trend is shown as a black line. The gray and purple bars represent respectively the winter and summer seasons on the X-axis. The height on the Y-axis corresponds to the amplitude of GL migration. Yellow triangles represent the maximum and minimum values of the grounding line in a given period.

Discussion

Our study confirmed the efficiency of satellite radar interferometry in detecting the position of the grounding line. This is the first such in-depth study, resulting in the position of the grounding line for such a long period (five years) and with such a frequency (every six days), achieved by combining SAR interferometry (Rignot *et al.* 2011) with CNN (Mohajerani *et. al.* 2021). The time needed to receive results for each 700×250 km wide interferogram settled around ten minutes, which took a week of processing in total. An attempt to manually locate and vectorize the position of the grounding line took us an hour and a half, which shows how automation improved the whole process. Satellite data allows high spatial coverage, while supporting DInSAR method with deep learning algorithms, allows receiving results in a relatively short time. That provides high

spatial and temporal resolution. The combination of frequent satellite revisits and rapid data processing makes it possible to obtain results continuously and at regular time intervals. It enables short-term monitoring of grounding line migration on an unprecedented scale, even week by week. With DInSAR method, the location of the grounding line can be determined with an accuracy up to 100 m (Rignot *et al.* 2011), depending on numerous factors, *e.g.*, bedrock topography, ice properties, and tidal amplitudes (Friedl *et al.* 2020). For comparison, accuracy of other tidal approaches settles around a kilometer or worse (Joughin *et al.* 2016; Dawson and Bamber 2017). The approach is independent of season, day, or weather conditions. There is also no need to take special measures to acquire the data, as they are freely available to anyone through online platforms.

The limitations of the approach were also verified during the study. A key aspect of radar interferometry is coherence, which is also the main issue in this field. There were some gaps in the fringe pattern continuity on the interferograms, which posed severe difficulties in grounding line delineation, often leading to breaks in the lines. The two main regions of interruption are presented on Fig. 7 by red rectangles. The most prominent issue concerns the place where the main tongue descends into the ocean (top red rectangle). Here, the velocity of the glacier's movement is usually high, and its vector is perpendicular to the position of the grounding line. In such places, the horizontal displacements caused by the glacier's flow are much larger than the vertical displacements caused by oceanic influences, making it impossible to effectively determine the boundary of ocean tides and thus, the position of the grounding line. High velocity also causes large decorrelation on interferograms, introducing additional noise in that zone. The situation is very similar in places where the glacier is fed by side streams (bottom red rectangle). These deficiencies are then

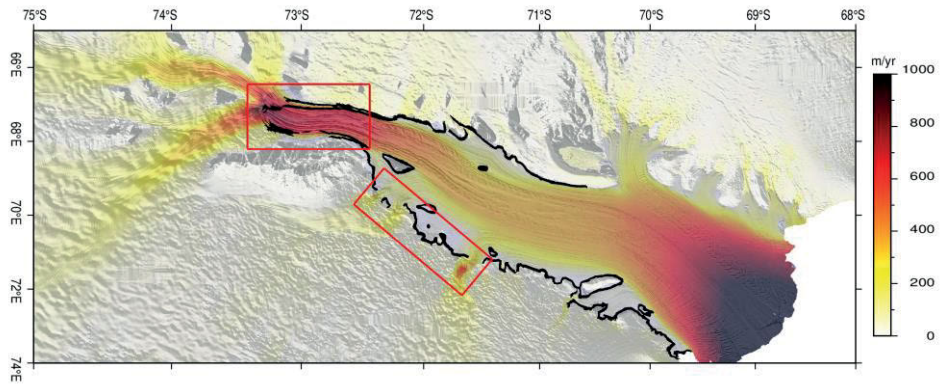

Fig. 7. Determined grounding lines (black lines) underlain by the mean ice masses velocity in 2018, based on the data from MEaSUREs project (Mouginot *et al.* 2017); WGS 84/Antarctic Polar Stereographic (EPSG:3031) coordinate system. Grounding line interruptions are marked with red rectangles.

related to glacier movement and the difficult characteristics of the selected area, which is a major curb in detecting the position of the grounding line with DInSAR method. Shorter temporal resolution can help increase the correlation between images, thereby improving coherence. Additionally, combining DInSAR method with offset-tracking techniques may also contribute.

Despite some regularities in trend and seasonality lines on the profiles, the results are characterized by large relative amplitudes and variability. They are dependent on numerous factors, which disturbs the relation between successive measurements. For example, acquisitions of SAR images are performed in various tidal states. Consequently, the interferograms take into account the vertical displacements resulting from the tidal amplitude over time. The tidal influence might be therefore responsible for the high relative variability of the obtained results, which is ostensibly random. That confirms the poor fit between trend lines and seasonality (Fig. 6; black and red lines respectively). However, it does not exclude the existence of other components in the obtained time series. Analyzing the divergence near the beginning of the floating ice, it was initially linked to poor coherence. However, the distribution of the grounding line is not random there, which rejects the above thesis. It has turned out that the results up until December 2018 are on the outer side of the glacier, while later measurements are on the inner side, which poses questions. The quality of the data and the processing were verified, and none showed irregularities. Thus, these results were considered correct and a consequence of unidentified phenomena or event.

It should also be mentioned here about the limitations in the reproduction of the results of the study, due to the way deep neural networks work. The development of CNNs has greatly accelerated since their first use. Despite describing the architecture in detail, they are increasingly used as a black-box tool, leading to a misapprehension of processes taking place inside the network. In practice, this means that the results of its work will be slightly different with each approach, even using the same input data. However, the resulting deviations are insignificant compared to the accuracy of the grounding line determination itself. Therefore, they are not important for performed analysis.

As mentioned earlier, the grounding line course is constantly shifting and is therefore often referred to as the grounding zone. It is a significant factor in modeling of basal melting, influencing the decrease of ice shelf's thickness, leading to increase in the velocity of ice streams feeding the shelf, and finally causing the retreat of the glacier (Seroussi and Morlighem 2018). The positions of the grounding lines depend on tidal and fluctuate in a relatively short period of time, *e.g.*, one month. Only multi-year time series observations allow identification of: (*i*) limits of the course of the grounding line in a specific area (grounding zones), (*ii*) seasonal changes in its course, and (*iii*) long-term trends in the movement of grounding lines. The aspects indicated above, combined with information on changes in the values of meteorological parameters, ice flow

velocities determined at exactly the same frequency using the offset-tracking technique, tides and other parameters over time, might provide complex monitoring of changes affecting the boundary between the ice sheet and the ice shelf. The tidal influence appears to be responsible for most of the signal shifts in the obtained time series. The current challenge is to extract the signal associated with tidal influence and other factors, which will allow more accurate observation of seasonality and long-term trend of grounding line position. A detailed understanding of the phenomena occurring in the grounding zone is crucial to the study of the Antarctic ice sheet, especially in view of current climate change.

Conclusion

This paper presents the potential of using satellite radar data and neural networks in quasi-automatic detection of grounding lines. The study area was the Amery Ice Shelf, and the analysis covered a period of five years. A data acquisition period of several days enabled the grounding line tracking at a very high temporal frequency (6/12 days). The DInSAR four-pass method was used to identify the position of the grounding line. Then, the calculated interferograms were processed by a 40-layer Convolutional Neural Network trained for grounding line detection. The results were validated based on available independent data for that area.

The grounding line position is dependent on numerous factors, *e.g.*, bedrock topography, ice properties and tidal amplitudes. However, it allows defining the grounding zone. In most cases the lines from the winter season are located closer to the land, while those from the summer season tend to cluster closer to the shelf. Frequency of grounding line detection might be used to accurately analyze short-term changes and seasonal patterns, although this will require extracting the signal related to mentioned phenomena. In addition, areas for which the determination of the grounding line in the proposed quasi-automatic mode was not possible were identified. According to the authors, the reason is the high speed of the glacier and the perpendicularity of the glacier's movement to the position of the grounding line. It appears mainly in areas where the main stream enters the ocean, causing phase decorrelation and additional noise. Combined with other data, *e.g.*, ice mass flow velocity and meteorological data, that will allow more comprehensive monitoring of changes occurring at the boundary between the ice shelf and the ice sheet on land.

Acknowledgements. — Calculations have been carried out using resources provided by Wroclaw Centre for Networking and Supercomputing (http://wcss.pl): grant No. 345. Reviewers are thanked for their valuable comments and corrections.

References

Anantrasirichai N., Biggs J., Albino F., Hill P. and Bull D. 2018. Application of machine learning to classification of volcanic deformation in routinely generated InSAR data. *Journal of Geophysical Research: Solid Earth* 123: 6592–6606. doi: 10.1029/2018JB015911

Avbelj J., Müller R. and Bamler R. 2015. A metric for polygon comparison and building extraction evaluation. *IEEE Geoscience and Remote Sensing Letters* 12: 170–174. doi: 10.1109/LGRS.2014.2330695

Bamber J.L., Gomez-Dans J.L. and Griggs J.A. 2009. A new 1 km digital elevation model of the Antarctic derived from combined satellite radar and laser data – Part 1: Data and methods. *The Cryosphere* 3: 101–111. doi: 10.5194/tc-3-101-2009

Bamler R. and Hartl P. 1998. Synthetic aperture radar interferometry. *Inverse Problems* 14: R1–R54. doi: 10.1088/0266-5611/14/4/001

Baumhoer C.A., Dietz A.J., Kneisel C. and Kuenzer C. 2019. Automated extraction of Antarctic glacier and ice shelf fronts from Sentinel-1 imagery using deep learning. *Remote Sensing* 11: 2529. doi: 10.3390/rs11212529

Brondex J., Gagliardini O., Gillet-Chaulet F. and Durand G. 2017. Sensitivity of grounding line dynamics to the choice of the friction law. *Journal of Glaciology* 63: 854–866. doi: 10.1017/jog.2017.51

Brunt K.M., Fricker H.A., Padman L., Scambos T.A. and O'Neel S. 2010. Mapping the grounding zone of the Ross Ice Shelf, Antarctica, using ICESat laser altimetry. *Annals of Glaciology* 51: 71–79. doi: 10.3189/172756410791392790

Budd W., Corry M. and Jacka T. 1982. Results from the Amery Ice Shelf Project. *Annals of Glaciology* 3: 36–41. doi: 10.3189/S0260305500002494

Catania G.A., Stearns L.A., Sutherland D.A., Fried M.J., Bartholomaus T.C., Morlighem M., Shroyer E. and Nash J. 2018. Geometric controls on tidewater glacier retreat in Central Western Greenland. *Journal of Geophysical Research: Earth Surface* 123: 2024–2038. doi: 10.1029/2017JF004499

Dawson G.J. and Bamber J.L. 2017. Antarctic grounding line mapping from CryoSat-2 radar altimetry. *Geophysical Research Letters* 44: 11886–11893. doi: 10.1002/2017GL075589

Floricioiu D., Krieger L., Chowdhury T.A. and Bässler M. 2021. *ESA Antarctic Ice Sheet Climate Change Initiative (AIS_cci): Grounding line location for key glaciers Antarctica 1994-2020, v2.0*. NERC EDS Centre for Environmental Data Analysis. Dataset available from https://catalogue.ceda.ac.uk/uuid/7b3bddd5af4945c2ac508a6d25537f0a

Fretwell P., Pritchard H.D., Vaughan D.G., Bamber J.L., Barrand N.E., Bell R., Bianchi C. *et al.* 2013. Bedmap2: improved ice bed surface and thickness datasets for Antarctica. *The Cryosphere* 7: 375–393. doi: 10.5194/tc-7-375-2013

Fricker H.A. and Padman L. 2006. Ice shelf grounding zone structure from ICESat laser altimetry. *Geophysical Research Letters* 33: L15502. doi: 10.1029/2006GL026907

Fricker H.A., Popov S., Allison I. and Young N. 2001. Distribution of marine ice beneath the Amery Ice Shelf. *Geophysical Research Letters* 28: 2241–2244. doi: 10.1029/2000GL012461

Fricker H.A., Allison I., Craven M., Hyland G., Ruddell A., Young N., Coleman R., King M., Krebs K. and Popov S. 2002. Redefinition of the Amery Ice Shelf East Antarctica grounding zone. *Journal of Geophysical Research: Solid Earth* 107: ECV1-1–ECV1-9. doi: 10.1029/2001JB000383

Fricker H.A., Coleman R., Padman L., Scambos T.A., Bohlander J. and Brunt K.M. 2009. Mapping the grounding zone of the Amery Ice Shelf East Antarctica using InSAR MODIS and ICESat. *Antarctic Science* 21: 515–532. doi: 10.1017/S095410200999023X

Fried M.J., Catania G.A., Stearns L.A., Sutherland D.A., Bartholomaus T.C., Shroyer E. and Nash J. 2018. Reconciling drivers of seasonal terminus advance and retreat at 13 central West

Greenland tidewater glaciers. *Journal of Geophysical Research: Earth Surface* 123: 1590–1607. doi: 10.1029/2018JF004628

Friedl P., Weiser F., Fluhrer A. and Braun M.H. 2020. Remote sensing of glacier and ice sheet grounding lines: A review. *Earth-Science Reviews* 201: 102948. doi: 10.1016/j.earscirev.2019.102948

Galton-Fenzi B., Maraldi C., Coleman R. and Hunter J. 2008. The cavity under the Amery Ice Shelf East Antarctica. *Journal of Glaciology* 54: 881–887. doi: 10.3189/002214308787779898

Goldstein R.M., Engelhardt H., Kamb B. and Frolich R.M. 1993. Satellite radar interferometry for monitoring ice sheet motion: Application to an Antarctic Ice Stream. *Science* 262: 1525–1530. doi: 10.1126/science.262.5139.1525

Gwyther D.E., Galton-Fenzi B.K., Dinniman M.S., Roberts J.L. and Hunter J.R. 2015. The effect of basal friction on melting and freezing in ice shelf–ocean models. *Ocean Modelling* 95: 38–52. doi: 10.1016/j.ocemod.2015.09.004

Hanssen R.F. 2001. *Radar Interferometry: Data Interpretation and Error Analysis*. Kluwer Academic, Dordrecht, Boston. doi: 10.1007/0-306-47633-9

Heaton J. 2020. *Applications of deep neural networks with Keras*. arXiv. doi: 10.48550/arXiv./2009.05673

Hogg A.E., Shepherd A., Gourmelen N. and Engdahl M. 2016. Grounding line migration from 1992 to 2011 on Petermann Glacier North-West Greenland. *Journal of Glaciology* 62: 1104–1114. doi: 10.1017/jog.2016.83

Holdsworth G. 1969. Flexure of a floating ice tongue. *Journal of Glaciology* 8: 385–397. doi: 10.3189/S0022143000026976

Horgan H.J. and Anandakrishnan S. 2006. Static grounding lines and dynamic ice streams: Evidence from the Siple Coast West Antarctica. *Geophysical Research Letters* 33: L18502. doi: 10.1029/2006GL027091

Horgan H.J., Christianson K., Jacobel R.W., Anandakrishnan S. and Alley R.B. 2013. Sediment deposition at the modern grounding zone of Whillans Ice Stream, West Antarctica. *Geophysical Research Letters* 40: 3934–3939. doi: 10.1002/grl.50712

Horgan H.J., Hulbe C., Alley R.B., Anandakrishnan S., Goodsell B., Taylor-Offord S. and Vaughan M.J. 2017. Poststagnation retreat of Kamb Ice Stream's grounding zone. *Geophysical Research Letters* 44: 9815–9822. doi: 10.1002/2017GL074986

Huang L., Luo J., Lin Z., Niu F. and Liu L. 2020. Using deep learning to map retrogressive thaw slumps in the Beiluhe region (Tibetan Plateau) from CubeSat images. *Remote sensing of environment* 237: 111534. doi: 10.1016/j.rse.2019.111534

Jacobel R.W., Robinson A.E. and Bindschadler R.A. 1994. Studies of the grounding-line location on Ice Streams D and E, Antarctica. *Annals of Glaciology* 20: 39–42. doi: 10.3189/1994AoG20-1-39-42

Joughin I., Smith B.E. and Holland D.M. 2010. Sensitivity of 21st century sea level to ocean-induced thinning of Pine Island Glacier, Antarctica. *Geophysical Research Letters* 37: L20502. doi: 10.1029/2010GL044819

Joughin I., Shean D.E., Smith B.E., and Dutrieux P. 2016. Grounding line variability and subglacial lake drainage on Pine Island Glacier, Antarctica. *Geophysical Research Letters* 43: 9093–9102, doi: 10.1002/2016GL070259

Krizhevsky A., Sutskever I. and Hinton G.E. 2017. ImageNet classification with deep convolutional neural networks. *Communications of the ACM* 60: 84–90. doi: 10.1145/3065386

Kussul N., Lavreniuk M., Skakun S. and Shelestov A. 2017. Deep learning classification of land cover and crop types using remote sensing data. *IEEE Geoscience and Remote Sensing Letters* 14: 5. doi: 10.1109/LGRS.2017.2681128

Lambrecht A., Mayer C., Hempel L., Nixdorf U. and Oerter H. 1997. Glaciological investigations in the grounding line area of the Foundation Ice Stream Antarctica. *Polarforschung* 65: 15–25. doi: 10013/epic.29738.d001

LeCun Y., Bengio Y. and Hinton G. 2015. Deep learning. *Nature* 521: 436–444. doi: 10.1038/nature14539

MacGregor J.A., Anandakrishnan S., Catania G.A. and Winebrenner D.P. 2011. The grounding zone of the Ross Ice Shelf, West Antarctica, from ice-penetrating radar. *Journal of Glaciology* 57: 917–928. doi: 10.3189/002214311798043780

Marsh O.J., Rack W., Floricioiu D., Golledge N.R. and Lawson W. 2013. Tidally induced velocity variations of the Beardmore Glacier, Antarctica, and their representation in satellite measurements of ice velocity. *The Cryosphere* 7: 1375–1384. doi: 10.5194/tc-7-1375-2013

Milillo P., Rignot E., Mouginot J., Scheuchl B., Morlighem M., Li X. and Salzer J.T. 2017. On the short-term grounding zone dynamics of Pine Island Glacier, West Antarctica, observed with COSMO-SkyMed interferometric data. *Geophysical Research Letters* 44: 10436–10444. doi: 10.1002/2017GL074320

Mohajerani Y., Jeong S., Scheuchl B., Velicogna I., Rignot E. and Milillo P. 2021. Automatic delineation of glacier grounding lines in differential interferometric synthetic-aperture radar data using deep learning. *Scientific Reports* 11: 4992. doi: 10.1038/s41598-021-84309-3

Mouginot J., Scheuchl B. and Rignot E. 2017. *MEaSUREs Annual Antarctic Ice Velocity Maps Version 1*. Data Set. NASA National Snow and Ice Data Center Distributed Active Archive Center (NSIDC DAAC), Boulder, Colorado. doi: 10.5067/9T4EPQXTJYW9

Porter C., Morin P., Howat I., Noh M.-J., Bates B., Peterman K., Keesey S. *et al*. 2018. *ArcticDEM Version 3*. Data set. Harvard Dataverse. doi: 10.7910/DVN/OHHUKH

Rignot E. 1996. Tidal motion ice velocity and melt rate of Petermann Gletscher, Greenland, measured from radar interferometry. *Journal of Glaciology* 42: 476–485. doi: 10.3189/S0022143000003464

Rignot E. and MacAyeal D. 1998. Ice-shelf dynamics near the front of the Filchner–Ronne Ice Shelf, Antarctica, revealed by SAR interferometry. *Journal of Glaciology* 44: 405–418. doi: 10.3189/S0022143000002732

Rignot E., Mouginot J. and Scheuchl B. 2011. Antarctic grounding line mapping from differential satellite radar interferometry. *Geophysical Research Letters* 38: L10504. doi: 10.1029/2011GL047109

Rignot E., Mouginot J., Morlighem M., Seroussi H. and Scheuchl B. 2014. Widespread rapid grounding line retreat of Pine Island Thwaites Smith and Kohler glaciers, West Antarctica, from 1992 to 2011. *Geophysical Research Letters* 41: 3502–3509. doi: 10.1002/2014GL060140

Rignot E., Mouginot J. and Scheuchl B. 2016. *MEaSUREs Antarctic Grounding Line from Differential Satellite Radar Interferometry Version 2*. Data Set. NASA National Snow and Ice Data Center Distributed Active Archive Center (NSIDC DAAC), Boulder, Colorado. doi: 10.5067/IKBWW4RYHF1Q

Rosen P.A., Hensley S., Joughin I.R., Li F.K., Madsen S.N., Rodriguez E. and Goldstein R.M. 2000. Synthetic aperture radar interferometry. *Proceedings of the IEEE* 88: 333–382. doi: 10.1109/5.838084

Rosenau R., Schwalbe E., Maas H.-G., Baessler M. and Dietrich R. 2013. Grounding line migration and high-resolution calving dynamics of Jakobshavn Isbræ, West Greenland. *Journal of Geophysical Research: Earth Surface* 118: 382–395. doi: 10.1029/2012JF002515

Rosier S.H.R., Gudmundsson G.H., King M.A., Nicholls K.W., Makinson K. and Corr H.F.J. 2017. Strong tidal variations in ice flow observed across the entire Ronne Ice Shelf and adjoining ice streams. *Earth System Science Data* 9: 849–860. doi: 10.5194/essd-9-849-2017

Sandwell D., Mellors R., Tong X., Wei M. and Wessel P. 2011. GMTSAR: An InSAR processing system based on Generic generic mapping tools. *Eos Transactions American Geophysical Union* 92: 234. doi: 10.1029/2011EO280002

Schild K.M. and Hamilton G.S. 2013. Seasonal variations of outlet glacier terminus position in Greenland. *Journal of Glaciology* 59: 759–770. doi: 10.3189/2013JoG12J238

Seroussi H. and Morlighem M. 2018. Representation of basal melting at the grounding line in ice flow models. *The Cryosphere* 12: 3085–3096. doi: 10.5194/tc-12-3085-2018

Stephenson S.N. 1984. Glacier flexure and the position of grounding lines: measurements by tiltmeter on Rutford Ice Stream, Antarctica. *Annals of Glaciology* 5: 165–169. doi: 10.3189/1984AoG5-1-165-169

Straneo F., Hamilton G.S., Stearns L.A. and Sutherland D.A. 2016. Connecting the Greenland Ice Sheet and the Ocean: A case study of Helheim glacier and Sermilik fjord. *Oceanography* 29: 34–45. doi: 10.5670/oceanog.2016.97

Tsai V. and Gudmundsson G. 2015. An improved model for tidally modulated grounding-line migration. *Journal of Glaciology* 61: 216–222. doi: 10.3189/2015JoG14J152

Uratsuka S., Nishio F. and Mae S. 1996. Internal and basal ice changes near the grounding line derived from radio-echo sounding. *Journal of Glaciology* 42: 103–109. doi: 10.3189/S0022143000030562

Vaughan D.G. 1994. Investigating tidal flexure on an ice shelf using kinematic GPS. *Annals of Glaciology* 20: 372–376. doi: 10.3189/1994AoG20-1-372-376

Weertman J. 1974. Stability of the Junction of an Ice Sheet and an Ice Shelf. *Journal of Glaciology* 13: 3–11. doi: 10.3189/S0022143000023327

Xie H., Chen L., Liu Shuang Jin Y., Liu J. and Liu Shijie Tong X. 2016. A least-squares adjusted grounding line for the Amery Ice Shelf using ICESat and Landsat 8 OLI data. *IEEE Journal of Selected Topics in Applied Earth Observations and Remote Sensing* 9: 5113–5122. doi: 10.1109/JSTARS.2016.2614758

Yu J., Liu H., Jezek K.C., Warner R.C. and Wen J. 2010. Analysis of velocity field mass balance and basal melt of the Lambert Glacier–Amery Ice Shelf system by incorporating Radarsat SAR interferometry and ICESat laser altimetry measurements. *Journal of Geophysical Research: Solid Earth* 115: 1–16. doi: 10.1029/2010JB007456

Zhang E., Liu L. and Huang L. 2019. Automatically delineating the calving front of Jakobshavn Isbræ from multitemporal TerraSAR-X images: a deep learning approach. *The Cryosphere* 13: 1729–1741. doi: 10.5194/tc-13-1729-2019

Received 20 December 2022
Accepted 11 July 2023